THE EFFECTS OF LONGITUDINAL RIBS ON ENTROPY GENERATION FOR LAMINAR FORCED CONVECTION IN A MICRO-CHANNEL

by

Nader POURMAHMOUD[a], Hosseinali SOLTANIPOUR[b*], and Iraj MIRZAEE[a]

[a] Department of Mechanical Engineering, Faculty of Engineering, Urmia University, Urmia, Iran
[b] Department of Mechanical Engineering, Urmia University of Technology, Urmia, Iran

Original scientific paper
DOI: 10.2298/TSCI130920110S

This paper deals with fluid flow, heat transfer, and entropy generation in an internally ribbed micro-channel. Mass, momentum, and energy equations for constant heat flux boundary condition are solved using the finite volume method. Average Nusselt number and Fanning friction factor are reported as a function of rib height at different Reynolds numbers. The effects of non-dimensional rib height, wall heat flux, and the Reynolds number on the entropy generation attributed to friction, heat transfer, and total entropy generation are explored. The first law indicates that rib height has the great effect on the flow filed and heat transfer. The second law analysis reveals that for any values of Reynolds number and wall heat flux, as rib height grows, the frictional irreversibility increases while, there is a rib height which provides the minimum heat transfer irreversibility. It is found that the optimum rib height with the minimum total entropy generation rate depends on Reynolds number and wall heat flux.

Key words: *entropy generation, irreversibility, non-dimensional heat flux, micro-channel, Reynolds number, rib*

Introduction

Micro-channel heat sinks are one of the essential parts of micro fluidic systems. In the recent years, fluid flow, heat transfer, and improving thermal performance of micro fluidic devices have become a crucial topic for researches. There are numerous studies on fluid flow and heat transfer in micro-channels as reviewed in [1-3]. Underlying understanding of the transport processes in micro-channel heat sinks has significant importance. Besides the investigations based on the basic conservation laws, the thermodynamics second-law analysis is a substantial point in optimum design of micro-channels. It is well known that, the lost available work is directly proportional to the entropy generation in a thermal system (Gouy-Stodola theorem). Hence, computation of the entropy generation related to the thermodynamic irreversibility is an important factor to determine the optimum operating conditions of thermal systems. Bejan [4] presented the methodology of computing entropy generation due to heat and fluid flow in thermal systems. He discussed on principles of the entropy generation minimization [5]. In another work, Bejan [6] explained the different reasons of entropy generation in applied thermal engineering. Hooman [7] studied entropy generation due to forced convection in microelectromechanical systems in the slip-flow regime. Expressions were proposed

* Corresponding author; e-mail: h.soltanipour@gmail.com

for the Bejan number and the entropy generation rate in terms of the Brinkman, Knudsen, and Prandtl numbers. Fully developed gaseous slip flow in trapezoidal silicon micro-channels was studied by Kuddusi [8]. The effects of rarefaction, aspect ratio, and viscous dissipation were explored. He stated that the dominant source of irreversibility in total irreversibility is a function of Brinkman number. Hung [9] focused on the viscous dissipation effect on entropy generation in fully developed forced convection of non-Newtonian fluid flow in circular micro-channels. He pointed out that based on Brinkman number and power-law index the viscous dissipation may have significant effect on entropy generation in micro-channels. Singh *et al.* [10] investigated the entropy generation due to flow and heat transfer in nanofluids. They analysed the effect of tube diameter and particle volume fraction on the entropy generation, and concluded that there is an optimum diameter with minimum entropy generation. Tabrizi and Seyf [11] numerically investigated the effect of using Al_2O_3-water nanofluids with different volume fractions and particle diameters on generated entropy of a tangential micro-heat sink. They concluded that the generated total entropy decreases with increasing volume fraction and Reynolds number and decreasing particles size. Ibanez and Cuevasb [12] performed the entropy generation analysis of an MHD flow in a parallel plate micro-channel. Based on the second law of thermodynamics, they determined the optimum operating conditions for specific values of the geometrical and physical parameters of the system. Analytical solution of forced convection and entropy generation in a uniformly heated micro-channel heat sink was carried out by Abbassi [13]. The effects of important parameters such as channel aspect ratio, thermal conductivity ratio, and porosity, on thermal and total entropy generation were reported. Yari [14] analytically studied the entropy generation for laminar flow in a micro-annulus. Various parameters such as Knudsen number, Brinkman number, annulus aspect ratio, and dimensionless temperature difference were taken into account. He showed that entropy generation lessens with increasing Knudsen number. Guo *et al.* [15-17] performed comprehensive studies on the entropy generation and thermodynamic performance of curved square micro-channels for laminar flow regime. The aim of the present paper is to investigate the entropy generation due to laminar forced convection in a ribbed micro-channel. The influences of non-dimensional wall heat flux, Reynolds number, and rib height on the entropy generation are explored. Optimum operating conditions based on the second law of thermodynamics are determined in terms of non-dimensional parameters.

Model description

The physical configuration of micro-channel is shown in fig. 1. According to the figure, four internal longitudinal ribs are mounted on micro-channel walls. All walls of micro-channel are subjected to external heat flux, q''. Because of symmetry, only a quarter of cross-section is simulated in this study as shown with dashed line in the figure. The width, H, and length, L, of the micro-channel are 200 μm and 120 mm, respectively. The thickness of rib and micro-channel walls denoted with, t_r, and t_w, are equal to 20 μm and 10 μm, respectively. The rib height is varied suitably to investigate its effect on thermal performance of micro-channel. Water is selected as the working fluid.

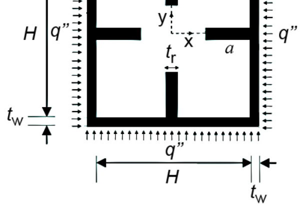

Figure 1. Geometry of micro-channel and ribs

The Reynolds and Nusselt numbers, Fanning friction factor, non-dimensional wall heat flux, and dimensionless rib height for the current problem are defined:

$$\mathrm{Re} = \frac{\rho V_{\mathrm{in}} H}{\mu} \tag{1}$$

$$\mathrm{Nu} = \frac{hH}{k_{\mathrm{f}}} \tag{2}$$

$$f = \frac{\Delta P}{2\rho V_{\mathrm{in}}^2} \frac{H}{L} \tag{3}$$

$$q^* = \frac{q'' H}{k_{\mathrm{f}} T_{\mathrm{in}}} \tag{4}$$

$$a^* = \frac{a}{H} \tag{5}$$

where V_{in} and T_{in} are the inlet velocity and temperature. Calculation is carried out for $0 \le a^* \le$ ≤ 0.45, $0.1 \le q^* \le 0.4$, and $600 \le \mathrm{Re} \le 1500$. It should be noted that $a^* = 0$, denotes no rib case or smooth micro-channel.

Governing equations and boundary conditions

In the present analysis, the following assumptions are made:

- the working fluid is Newtonian,
- the transport process considered as steady flow,
- the fluid has constant properties and flow is laminar,
- the Brinkman numbers calculated in this problem are less than unity, hence the viscous dissipation effect is neglected [18, 19], and
- the effect of gravity is negligible in momentum equation for the fluid flow in micro-channels [20, 21].

Using the following non-dimensional parameters:

$$x^* = \frac{x}{H}, \quad y^* = \frac{y}{H}, \quad z^* = \frac{z}{H}, \quad \vec{V}^* = \frac{\vec{V}}{V_{\mathrm{in}}}, \quad P^* = \frac{P}{\rho V_{\mathrm{in}}^2},$$

$$T^* = \frac{T - T_{\mathrm{in}}}{T_{\mathrm{in}}}, \quad \nabla^* = H\nabla, \quad \mathrm{Pr} = \frac{\mu C_p}{k_{\mathrm{f}}}$$

The dimensionless continuity, Navier-Stokes and energy equations in the Cartesian co-ordinate system are:

$$\nabla^* \vec{V}^* = 0 \tag{6}$$

$$\vec{V}^* \nabla^* \vec{V}^* = -\nabla^* P^* + \frac{1}{\mathrm{Re}} \nabla^{*2} \vec{V}^* \tag{7}$$

$$\vec{V}^* \nabla^* T^* = \frac{1}{\mathrm{Re\,Pr}} \nabla^{*2} T^* \tag{8}$$

and energy equation in solid regions:

$$\nabla^{*2} T_s^* = 0 \tag{9}$$

where the starred variables are dimensionless ones, P is the pressure, T – the temperature, and $\vec{V}$ – the velocity vector, respectively.

The non-linear governing equations of the problem are subjected to following boundary conditions.

At the micro-channel inlet, uniform axial velocity, V_{in}, and temperature, T_{in}, are specified:

$$V_x^* = V_y^* = 0, \qquad V_z^* = 1, \qquad T^* = 0 \tag{10}$$

At the outlet, the pressure outlet boundary condition is employed. At micro-channel walls, constant heat flux is specified:

$$q^* = -\nabla^* T^* \vec{n} \tag{11}$$

where $\vec{n}$ is the unit vector normal to microchannel walls.

At solid and fluid interface, no slip boundary condition is set for velocity components, whereas, temperature between solid and liquid is coupled to allow for conjugate heat transfer. The normal velocity component at the symmetry plane is zero. Moreover, there is no diffusion flux across the symmetry plane, therefore the normal gradients of all flow variables is zero.

After solving the governing equations, the volumetric entropy generation due to the heat transfer irreversibility, S'''_{T}, fluid frictional irreversibility, S'''_{f}, and total entropy generation, S'''_{gen}, are expressed [4]:

$$S'''_{\mathrm{T}} = \frac{k}{T^2} \left| \nabla T \right|^2 \tag{12}$$

$$S'''_{\mathrm{f}} = \frac{\mu}{T} \varphi \tag{13}$$

$$S'''_{\mathrm{gen}} = S'''_{\mathrm{f}} + S'''_{\mathrm{T}} \tag{14}$$

where φ is the viscous dissipation function given by:

$$\varphi = 2\left[\left(\frac{\partial V_x}{\partial x}\right)^2 + \left(\frac{\partial V_y}{\partial y}\right)^2 + \left(\frac{\partial V_z}{\partial z}\right)^2\right] + \left[\left(\frac{\partial V_x}{\partial y} + \frac{\partial V_y}{\partial x}\right)^2\right] +$$
$$+ \left\{\left(\frac{\partial V_y}{\partial z} + \frac{\partial V_z}{\partial y}\right)^2 + \left[\left(\frac{\partial V_x}{\partial z} + \frac{\partial V_z}{\partial x}\right)^2\right]\right\} - \frac{2}{3}\nabla\vec{V} \tag{15}$$

The Bejan number is the important parameter, which represents the contribution of entropy generation due to heat transfer on total entropy generation, which is defined:

$$\mathrm{Be} = \frac{S'''_{\mathrm{T}}}{S'''_{\mathrm{f}}} \tag{16}$$

It is clear that Bejan number varies from 0 to 1. Be > 0.5 means that heat transfer irrevesibility is the dominate term in total irreversibility while Be < 0.5 implies that frictional irreversibility is greater than heat transfer irreversibility. A Bejan number of Be = 0.5 represents that entropy generation due to heat transfer and friction have the same contribution on total entropy generation.

Numerical approach and grid study

Governing eqs. (6)-(9) are solved by the finite volume based SIMPLE approach [22] with first-order upwind scheme for the convection and central differencing for the diffusion terms on a staggered grid. A convergence criteria of 10^{-9} is used for all calculations. In order to ensure grid independency, three uniform grid sizes are submitted to an extensive testing of results. Comparison of different grid system results (for total entropy generation rate in the case of Re = 1500, q^* = 0.2, and a^* = 0.4) is shown in tab. 1. It is observed that the predicted total entropy generation rate are changed by 2% from the first to the second mesh, and only by 0.27% upon further refinement to the third grid. Consequently, the grid system with 24 × 24 × 400 nodal points (24 × 24 on the *x*-*y* plane and 400 nodes along the *z*-direction) is adopted in this study.

Table 1. Grid independency test

Grid size	Total entropy generation rate
12 × 12 × 400	0.0538
24 × 24 × 400	0.0549
48 × 48 × 400	0.0551

Validation

To verify the accuracy of present results, we compared numerical results with experimental data of Liu *et al.* [23]. In the experiments, they used a rectangular micro-channel with length 20 mm and aspect ratio of 15. The comparison is illustrated in fig. 2, wherein the variation of the average Nusselt number as a function of Reynolds number is presented. As shown in fig. 2, the predicted Nusselt numbers demonstrate good agreement with the measured data.

Results and discussions

The effect of Reynolds number

In this section, we present the effect of Reynolds number on flow characteristics, heat transfer, and entropy generation. It should be mentioned that in this section, non-dimensional wall heat flux is kept constant at q^* = 0.2. Figure 3 plots the Fanning friction factor as a function of non-dimensional rib height at different Reynolds numbers. It is evident from figure that Fanning friction factor increases with rise of rib height, since the growth of rib height leads to increase of pressure drop.

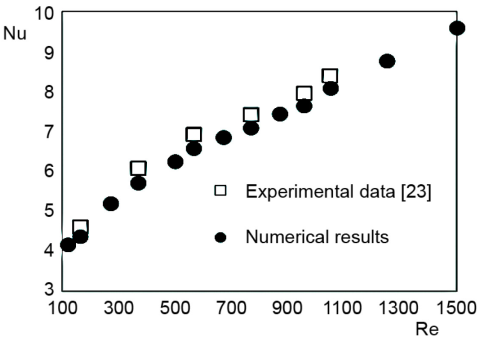

Figure 2. Comparison of the present results with experimental data

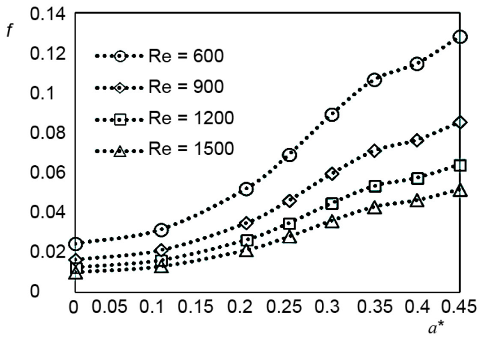

Figure 3. Effect of rib height on Fanning friction factor

The effects of rib height on the average Nusselt number at different Reynolds number are depicted in fig. 4. This figure clearly exhibits that the use of ribs, augments con-

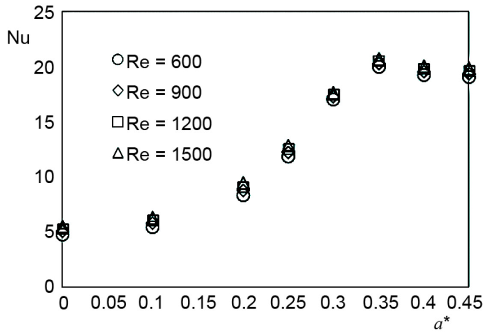

Figure 4. Effect of rib height on the Nusselt number

siderably the Nusselt number. An interesting result of this figure is that for $a^* < 0.35$, the Nusselt number increases with growth of rib height and reaches to its maximum value at $a^* = 0.35$ and then decreases. This result is close to the one obtained by Foong *et al.* [24]. They determined the optimum fin height ratio of 0.335.

It would be more practical to determine the entropy generation rate in non-dimensional form. The non-dimensional entropy generation rate in the whole micro-channel are defined by [25]:

$$S_{\mathrm{f}}^{*} = \frac{\int S_{\mathrm{f}}''' \, \mathrm{d}\forall}{\dfrac{\dot{Q}}{T_{\mathrm{in}}}} \tag{17}$$

$$S_{\mathrm{T}}^{*} = \frac{\int S_{\mathrm{T}}''' \, \mathrm{d}\forall}{\dfrac{\dot{Q}}{T_{\mathrm{in}}}} \tag{18}$$

$$S_{\mathrm{gen}}^{*} = \frac{\int S_{\mathrm{gen}}''' \, \mathrm{d}\forall}{\dfrac{\dot{Q}}{T_{\mathrm{in}}}} \tag{19}$$

where the integration is performed over the volume of fluid and solid regions and $\dot{Q}$ is the heat transfer rate from the walls.

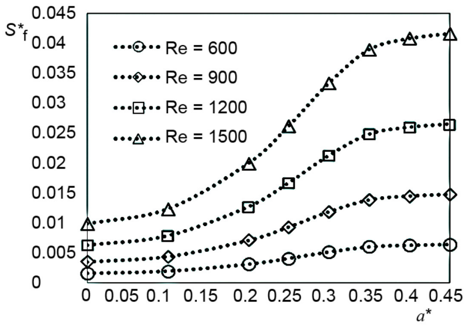

Figure 5. Variation of S_{f}^{*} with rib height

The variation of frictional entropy generation *vs.* the non-dimensional rib height at different Reynolds numbers is shown in fig. 5. At specified rib height, the value of S_{f}^{*} increases with the rise of Reynolds number. This is due to the fact, that frictional irreversibility is related to velocity gradients, which is larger at high Reynolds numbers. Another feature of fig. 5 is that for the same Reynolds number, S_{f}^{*} increases as non--dimensional rib height grows, because of increased solid surfaces.

Figure 6 indicates the values of entropy generation due to heat transfer irreversibility for non-dimensional rib height ranging from 0-0.45. As expected, when heat transfer coefficient (or Nusselt number) increases, the temperature gradient in the flow field becomes milder, which leads to lower heat transfer irreversibility. Consequently, Nu – a^* and S_{T}^{*} – a^* curves should have the opposite trends. This is evident by comparison of figs. 4 and 6. As a result, regardless of Reynolds number, $a^* = 0.35$ provides the minimum value of heat transfer irreversibility.

Figure 7 illustrates the variation of Bejan number against a^* for various Reynolds numbers. It is clear from the figure that for the range of $0.25 \le a^* \le 0.45$ and $900 \le \mathrm{Re} \le 1500$, the Bejan number is less than 0.5, indicating that for these cases the frictional irreversibly is the dominate term in total irreversibility.

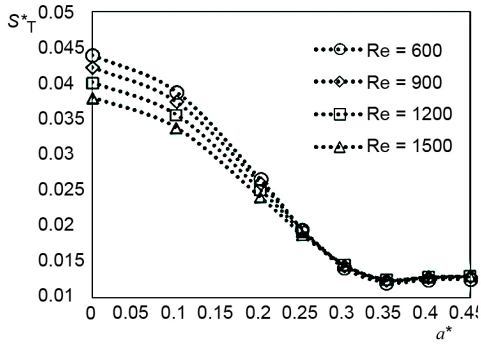

Figure 6. Variation of S_T^* with rib height

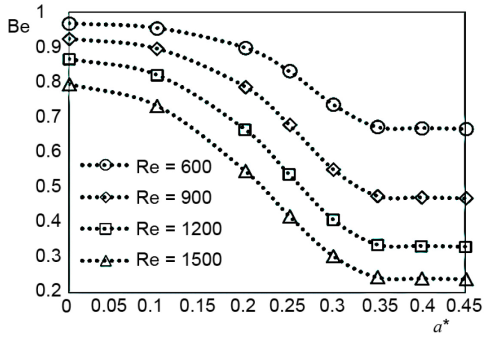

Figure 7. Variation of Bejan number with rib height

As previously mentioned, when rib height increases, frictional entropy generation decreases. On the other hand, entropy generation due to heat transfer decreases as rib height grows. The presence of these competing effects makes it possible to have an optimum rib height, which minimizes the total entropy generation rate. Figure 8 shows the variation of S_{gen}^* with a^*. The figure clarifies that for any Reynolds Number, there is a rib height with the minimal total entropy generation rate, which based on the second law of thermodynamics has the best thermal performance.

Figure 9 shows the optimum rib height as a function of Reynolds number. It is observed that at high Reynolds number small rib sizes provide the optimal operating condition based on second law. These results provide worthwhile information for the micro-channel design.

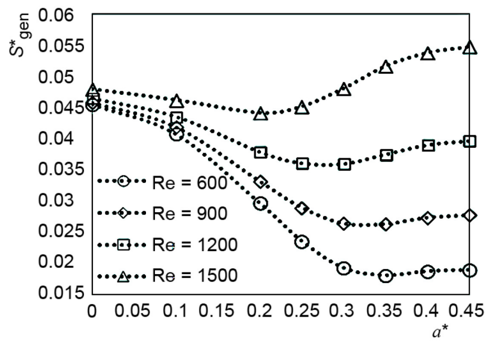

Figure 8. Variation of S^*_{gen} with rib height

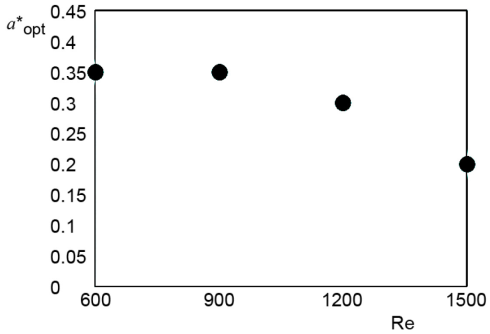

Figure 9. Optimum rib height against Reynolds number for $q^* = 0.2$

The effect of non-dimensional heat flux

In this section, we present the effect of heat flux on entropy generation. It should be noted that in this section, the Reynolds number is kept constant and equals to 1200. The effects of non-dimensional wall heat flux on S_{f}^*, S_{T}^*, and S_{gen}^* are shown in figs. 10, 11, and 12, respectively. A clear trend can be found from the fig. 10, that for all rib heights, S_f^* decreases as q^* increases, because there is the temperature term in the denominator of eq. (13).

Figure 11 shows the variation of S_T^* with rib height. It is obvious that for all non-dimensional heat flux considered in this study the irreversibility due to the heat transfer is minimal for $a^* = 0.35$. As expected, for specified rib height, S_T^* rises as q^* increases.

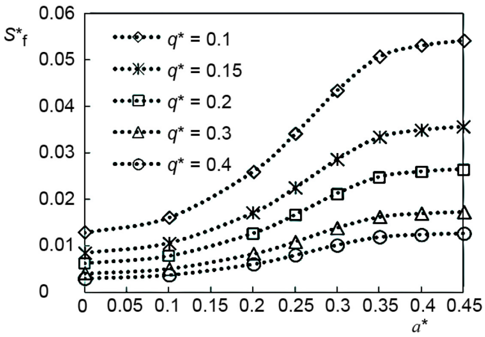

Figure 10. Effects of *q on entropy generation induced by friction**

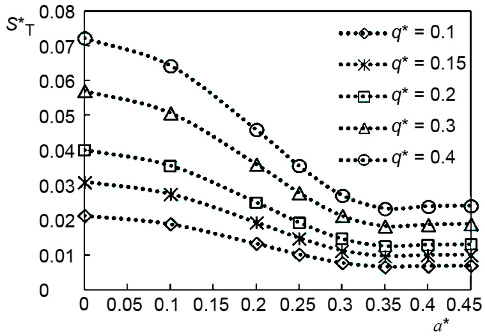

Figure 11. Effects of *q on entropy generation induced by heat transfer**

Figure 12 shows the variation of S_{gen}^* with rib height at different wall heat fluxes. At low heat fluxes, total entropy generation rises as the rib height increases indicating that for this cases, frictional entropy generation is the dominate term in total entropy generation. Nevertheless, at higher heat fluxes there is a rib height with minimum total entropy generation, which depends on wall heat flux. It is interesting to observe from the figure that for $a^* \geq 0.2$, for any rib height, there is an optimum non-dimensional heat flux, which provides the least total entropy generation rate.

Figure 13 depicts the optimum rib height *vs.* non-dimensional wall heat flux. The figure exhibits that the optimal rib height increases as non-dimensional rib size increases.

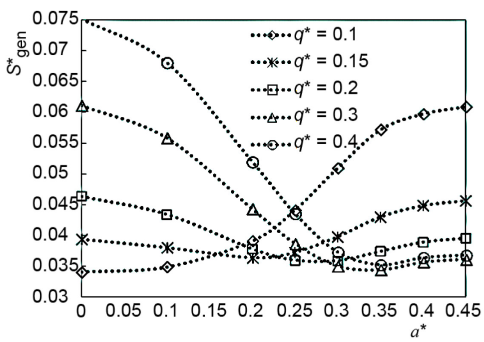

Figure 12. Effects of *q on total entropy generation**

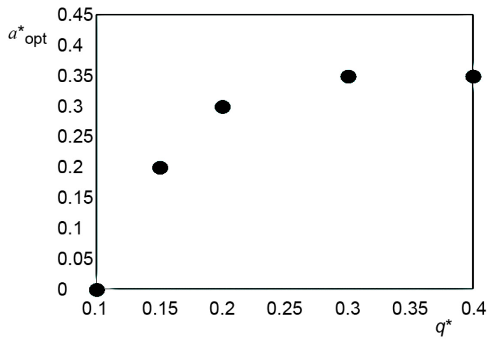

Figure 13. Optimum rib height against non-dimensional wall heat flux for Re = 1200

Conclusion

Laminar forced convection of water flow in an internally ribbed micro-channel is analysed from both the first and second law points of view. The effects of three different parameters *i. e.*, Reynolds number, non-dimensional wall heat flux, and dimensionless rib height on entropy generation is presented. Numerical results show that regardless of Reynolds number and wall heat flux, a rib height of $a^* = 0.35$ provides the maximum Nusselt number and minimum heat transfer irreversibility. Based on the second law of thermodynamics and minimal entropy generation principle, the optimum rib height is obtained as a function of Reynolds number and non-dimensional wall heat flux. These results can assist in improving and optimizing of micro-channel thermal performance.

Nomenclature

a – rib height, [m]
c_p – specific heat, [Jkg^{-1}K^{-1}]
f – Fanning friction factor, [–]
H – width of the micro-channel, [μm]
h – heat transfer coefficient, [Wm^{-2}K^{-1}]
k – thermal conductivity, [Wm^{-1}K^{-1}]
L – length of the micro-channel, [m]
P – pressure, [Nm^{-2}]
Pr – Prandtl number, [–]
$\dot{Q}$ – heat transfer rate, [W]
q'' – heat flux, [Wm^{-2}]
Re – Reynolds number, [–]
T – temperature, [K]
V – velocity
$\vec{\mathrm{V}}$ – velocity vector
$\forall$ – volume, [m^3]

Greek symbols

μ – dynamic viscosity, [Nsm^{-2}]
ρ – density, [kgm^{-3}]
φ – viscous dissipation, [s^{-2}]

Subscripts

in – inlet
f – fluid
r – rib
s – solid
w – wall

References

[1] Garimella, S. V., Sobhan, C. B., Transport in Microchannels – a Critical Review, *Annu. Rev. Heat Transfer, 13* (2003), 3, pp. 1-50
[2] Hassan, I., *et al.*, Microchannel Heat Sinks: an Overview of the State-of-the-Art, *Microscale Thermal Engineering, 8* (2004), 3, pp. 183-205
[3] Adham, A. M., *et al.*, Thermal and Hydrodynamic Analysis of Microchannel Heat Sinks: A Review, *Renewable and Sustainable Energy Reviews, 21* (2013), May, pp. 614-622
[4] Bejan, A., *Entropy Generation through Heat and Fluid Flow*, John Wiley and Sons, New York, USA, 1982
[5] Bejan, A., *Entropy Generation Minimization*, CRC Press, Boca Raton, Fla., USA, 1996
[6] Bejan, A., Second-Law Analysis in Heat Transfer and Thermal Design, *Advances in Heat Transfer, 15* (1982), Dec., pp. 1-58
[7] Hooman, K., Entropy Generation for Microscale-Forced Convection: Effects of Different Thermal Boundary Conditions, Velocity Slip, Temperature Jump, Viscous Dissipation, and Duct Geometry, *International Communications in Heat and Mass Transfer, 34* (2007), 8, pp. 945-957
[8] Kuddusi, L., First and Second Law Analysis of Fully Developed Gaseous Slip Flow in Trapezoidal Silicon Microchannels Considering Viscous Dissipation Effect, *International Journal of Heat and Mass Transfer, 54* (2011), 1, pp. 52-64
[9] Hung, Y. M., Viscous Dissipation Effect on Entropy Generation for Non-Newtonian Fluids in Microchannels, *International Communications in Heat and Mass Transfer, 35* (2008), 9, pp. 1125-1129
[10] Singh, P. K., *et al.*, Entropy Generation Due to Flow and Heat Transfer in Nanofluids, *International Journal of Heat and Mass Transfer, 53* (2010), 21, pp. 4757-4767
[11] Tabrizi, A. Sh., Seyf, H. R., Analysis of Entropy Generation and Convective Heat Transfer of Al_2O_3 Nanofluid Flow in a Tangential Micro Heat Sink, *International Journal of Heat and Mass Transfer, 55* (2012), 15-16, pp. 4366-4375
[12] Ibaneza, G., Cuevasb, S., Entropy Generation Minimization of a MHD (Magnetohydrodynamic) Flow in a Microchannel, *Energy, 35* (2010), 10, pp. 4149-4155
[13] Abbassi, H., Entropy Generation Analysis in a Uniformly Heated Microchannel Heat Sink, *Energy, 32* (2007), 10, pp. 1932-1947
[14] Yari, M., Second-Law Analysis of Flow and Heat Transfer Inside a Microannulus, *International Communications in Heat and Mass Transfer, 36* (2009), 1, pp. 78-87

[15] Guo, J., *et al.*, Second Law Analysis of Curved Rectangular Channels, *International Journal of Thermal Sciences, 50* (2011), 5, pp. 760-768
[16] Guo, J., *et al*., The Effect of Temperature-Dependent Viscosity on Entropy Generation in Curved Square Microchannel, *Chemical Engineering and Processing: Process Intensification*, *52* (2012), Feb., pp. 85-91
[17] Guo, J., *et al*., Viscous Dissipation Effect on Entropy Generation in Curved Square Microchannels, *Energy, 36* (2011), 8, pp. 5416-5423
[18] Tso, C. P., Mahulikar, S. P., The Use of the Brinkman Number for Single Phase Forced Convective Heat Transfer in Microchannels, *International Journal of Heat and Mass Transfer, 41* (1998), 12, pp. 1759-1769
[19] Tso, C. P., Mahulikar, S. P., The Role of the Brinkman Number in Analyzing Flow transitions in Microchannels, *International Journal of Heat and Mass Transfer, 42* (1999), 10, pp. 1813-1833
[20] Dang, T., *et al.*, A Study on the Simulation and Experiment of a Microchannel Counter-Flow Heat Exchanger, *Applied Thermal Engineering, 30* (2010), 14-15, pp. 2163-2172
[21] Dang, T., *et al*., Influence of Gravity on the Performance Index of Microchannel Heat Exchangers – Experimental Investigations, *Proceedings,* World Congress on Engineering, London, UK, 2011, pp. 2094-2099
[22] Patankar, S. V., *Numerical Heat Transfer and Fluid Flow*, Hemisphere, Washington, D.C., 1980
[23] Liu, Ch., *et al.*, Experimental Investigations on Liquid Flow and Heat Transfer in Rectangular Microchannel with Longitudinal Vortex Generators, *International Journal of Heat and Mass Transfer, 54* (2011), 13-14, pp. 3069-3080
[24] Foong, A. J. L., *et al*., Laminar Convective Heat Transfer in a Microchannel with Internal Longitudinal Fins, *International Journal of Thermal Sciences, 48* (2009), 10, pp. 1908-1913
[25] Hesselgreaves, J. E, Rationalisation of Second Law Analysis of Heat Exchangers, *International Journal of Heat Mass Transfer, 43* (2000), 22, pp. 4189-4204

Paper submitted: September 20, 2013
Paper revised: July 3, 2014
Paper accepted: July 6, 2014